International Journal of Disaster Risk Reduction 120 (2025) 105391

Contents lists available at ScienceDirect

International Journal of Disaster Risk Reduction

journal homepage: www.elsevier.com/locate/ijdrr

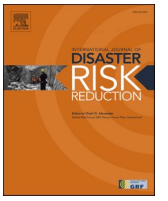

Multiple hazards and exposure in California: A space-time analysis of temperature, drought, and wildfire

Erin Shives [a,b,*,1], Tzu-Hsin Karen Chen [a,c,d], C. Karen Seto [a]

[a] Yale School of the Environment, Yale University, New Haven, CT, 06511, USA
[b] Massachusetts Institute of Technology, Cambridge, MA, USA
[c] Department of Urban Design and Planning, University of Washington, Seattle, WA, USA
[d] Department of Environmental and Occupational Health Sciences, University of Washington, Seattle, WA, USA

ARTICLE INFO

Keywords:
Natural hazards
California
Exposure
Spatiotemporal
Multiple hazards
Climate change

ABSTRACT

Natural hazards sharing climatic precursors of temperature and precipitation– heat, drought, and wildfires–amplify their individual effects when they occur in the same time and space. Their combined effects pose numerous challenges to urban areas by decreasing resilience of infrastructure, affecting people's health and safety, and undermining economic stability. This study quantifies the temporal and spatial interactions between heat, drought, and wildfires in California's Metropolitan Statistical Areas for the month of July from 1981 to 2022. We aim to address two questions: 1) How are these hazards changing over time and space? And 2) How are these hazards combined exposing the local land and populations? The temporal analysis found each individual hazard is increasing in frequency. The annual average values for maximum temperature and wildfire burn areas measure consistently above their 20th-century average and drought above the 40-year average. Since 2000, each hazard measured higher than their long-term averages for almost every year, underscoring the persistent climate strain on the state. The spatial assessment revealed, from 1981 to 2022 for the month of July, one-third of California has experienced multiple hazard events encompassing temperature, drought, and/or wildfire. Comparison between population exposure and land (% area) exposure reveals that Riverside experienced the highest total population exposed to multiple hazards, over 2 million people, despite less than 30 % of its land exposed to multiple hazards. The results indicate urbanization has further amplified vulnerabilities and comprehensive data regarding multiple hazards and types of exposure are necessary to estimate risk for public health and economy.

1. Introduction

Natural hazards are becoming more frequent and unpredictable, increasing the likelihood for multiple hazards to overlap in a given time and space [5,48]. Specifically natural hazards, such as wildfires or drought, do not often occur alone [28]. More often, they occur together with another natural hazard that share common climatic precursors [4,52]. Multi-hazard occurrences can happen at the same time (compounding) or following one after the next (cascading) (Fig. 1) [19,28,55]. Compounding events are when two or more natural hazards occur concurrently with underlying conditions such that it amplifies the impact when these events occur within the

* Corresponding author. Yale School of the Environment, Yale University, New Haven, CT, 06511, USA.
E-mail addresses: shiveserin@gmail.com (E. Shives), kthchen@uw.edu (T.-H.K. Chen), karen.seto@yale.edu (C.K. Seto).
[1] Present address: 64 Prentiss St. Apt 3 Cambridge, MA 02140.

https://doi.org/10.1016/j.ijdrr.2025.105391
Received 6 September 2024; Received in revised form 11 March 2025; Accepted 12 March 2025
Available online 13 March 2025

same timeframe and region [38,52,64]. Cascading events are when two or more natural hazards occur consecutively, with the first event amplifying the adverse effects of weather conditions such that it can trigger a following event [22,56]. Multiple hazard events pose higher risk to their surrounding environments because their cumulative effects can have more detrimental impacts than individual events [34,56].

The occurrence of multiple hazards in a given time and space not only impacts the environmental conditions but contributes to societal risk [16,22,42]. When these hazards occur at the same location, their cumulative impact can escalate their effects compared to when they occur alone [38,52,64]. For example, observed increases in drought across California have contributed to extended wildfire seasons [7]. Between 2017 and 2020, these prolonged wildfire seasons claimed 200 lives and destroyed 45,000 structures, with smoke and extreme air pollution affecting millions [11]. In 2020 alone, the total economic losses are estimated to exceed $19 billion [49]. And in January of 2025, wildfires spread across the Los Angeles region in Southern California, resulting in damages estimated to cost near $250 billion [29]. Two of these wildfires, the Eaton Fire and Palisades Fire, have been recorded as the second and third most destructive in the history of the state [39]. As temperature and precipitation patterns are projected to shift around the world, understanding the local interaction of hazards is critical for sustaining resilient cities [34,53].

More than 4.2 billion people around the world live in urban areas which encompass complex infrastructure, dense populations, and dynamic economies [34,35,47]. As cities expand, they may create additional hazard risks, such as adding buildings as fuel at the wildfire-urban interface [50]. Many urban areas are exposed to one or more natural hazards; hazards pose a risk to these complex systems because climatic disruptions can expose their vulnerabilities and lead to devastating consequences [34,45]. Since 1990, the impact of natural hazards has caused 1.6 million deaths globally and an overall economic loss ranging between 260 and 320 USD per year [60]. The IPCC 6th Assessment Report calls for the implementation of multiple hazards into risk assessments because of the vulnerabilities that exist in urban infrastructure, public health and safety, and sensitive economies [4,5,30,45]. Ongoing expansion of urban areas will continue to increase their exposure to individual hazards and/or multiple hazards, leading to more risk and potential consequences that can exacerbate existing vulnerabilities [26,34,60].

In this study, we aim to address two research questions: 1) How are these hazards changing over time and space? And 2) How are these hazards combined exposing the local land and populations? These questions aim to understand how these hazards have individually changed over time and space and provide insight into potential vulnerabilities and guiding risk reduction efforts.

We analyze two key types of exposure in urban areas, land (% area) exposure and population exposure, helping understand which is most at risk from multiple hazards [26,55]. Knowing the extent of land exposure is crucial due to the economic assets concentrated in and around urban areas, including: densely built infrastructure, transportation networks, agricultural zones, and energy production facilities [34]. In addition, recognizing the amount of population exposed is critical for safeguarding public health and safety, as significant disruptions can cascade into adverse impacts to people's lives as well as undermine economic stability [37,61]. Land exposure and population exposure often overlap. However, identifying the level of multiple hazard exposure for both helps clarify where to focus resources for risk assessments. This approach supports better allocation of resources and more effective mitigation of vulnerabilities.

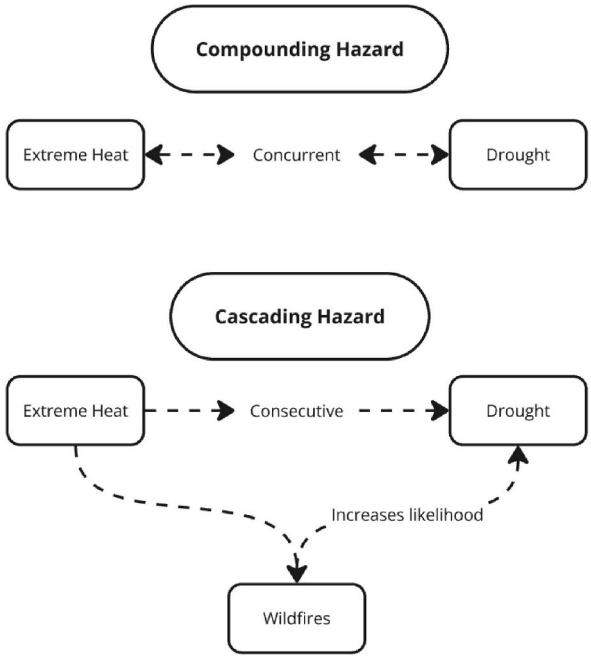

Fig. 1. The relationship of compounding and cascading hazards between extreme heat, drought, and/or wildfires.

2. Study area

California is the United States's largest economy, earning its status from sectors in agriculture, entertainment, recreation, technology, and trade [8,15]. Our study area includes 26 Metropolitan Statistical Areas (MSAs) encompassing large areas with populations exceeding 50,000, bridging the urban sector with the surrounding land that those urban areas rely on for their economic well-being (Fig. 2). Across the state exist dense clusters of urban populations, accounting for around 12 % of the U.S. population, which rely directly on their surrounding land to support their local economies and livelihoods (See Appendix A.1 California Population per sq. mile by Census Tract for 2020) [8,15]. The state is known for its diverse landscapes of coastal shorelines, agricultural land, mountain ranges and deserts which are categorized into 11 Modified Köppen Climate Classifications, including: Semi-arid, steppe (hot); Semi-arid, steppe; Semi-arid, steppe with summer fog; Arid low latitude desert (hot); Arid mid latitude desert; Mediterranean/hot summer; Mediterranean/cool summer; Mediterranean/summer fog; Cool continental/dry summer; Cold winter/dry summer; and Highland/Timberline [12].

Characterized as one of the most "climate-challenged" regions in the United States, California is projected to be at greatest risk to climate-induced hazards due to high exposure and vulnerability [8,35,38]. In 2023, the state experienced 28 separate billion-dollar weather and climate related disaster events, totaling at 92.9 billion USD [40]. Three of the most notorious hazards affecting California are extreme temperatures, severe drought, and uncontrollable wildfires with each individually contributing negative impacts across urban areas [6,36,44]. For example, an individual hazard, such as extreme temperature, can amplify the underlying effects of decreasing soil moisture, thereby increasing drought conditions which depletes the landscape creating greater potential for wildfire occurrence [5]. Each of these hazards have different timelines and spatial distributions which makes cumulative impact more difficult to predict [10,23,51].

Heat events, prolonged high temperatures or perceived heat conditions that exceed typical norms for a given region, impact the populations in California, especially those residing and working in highly urbanized areas. Extended periods of extreme heat correlate with hospital visits due to heat exhaustion, strokes, and heat-related mortality; from 1999 to 2009, 19 heat-related events occurred and resulted in 11,000 excess hospitalizations [8]. By mid-century, Central Valley is expected to experience two weeks longer of heat-related events [8]. In NOAA's weather and climate related economic impact reports, heat is not considered which does not accurately reflect California's allocation of funding towards handling this hazard [40]. With the current health-related risks and projected increases in heat, this carries direct implications for government mitigation strategies.

In many situations, heat events increase the occurrence of drought within surrounding areas; together their effects contribute to landscape degradation, resulting in crop loss and major disruptions to the supply chain and economic stability [30,32]. The 2021 drought cost the agriculture sector nearly 1.1 billion USD and 8750 jobs [30]. The extent of damage across California's landscape in 2021 from combined heat and drought impact directly contributed to the extent of wildfire spread, burning roughly the size of San

Fig. 2. Map of California displaying study area terrain and Metropolitan Statistical Areas (MSA) boundaries in black.

Diego County at 2.5 million acres [14].

California's 4th Climate Change Assessment evaluates the state's current and future impacts of each of these hazards individually but does not account for the combined effects in co-occurring hazard events [8]. The combined impact of these three hazards results in land and population exposure with a combined loss through public health and economy. Government agencies seek to use historic multiple hazard assessments as a tool to mitigate the impacts to local population and sustainable planning and development [8,33]. While other studies have looked at spatiotemporal relationships with wildfire in California [9,63], this study is unique as this is the first study to analyze the spatiotemporal clustering of extreme heat, drought, and wildfires in California at high resolution, in addition to assessing their relation to land exposure and population exposure across the MSAs.

In this study, we examine heat by temperature maximum (Tmax), drought by the Palmer Drought Severity Index (PDSI), and wildfire by total burnt area, to observe their co-occurrences based on their temporal and spatial history from 1981 to 2022. We use California's MSAs to then assess their relation to land exposure and population exposure. July is used as the base month for this analysis because all three hazards are at their collective highest impact during this time of year. For each hazard, we seek to understand the frequency change, combined spatial distribution and overlap, and which MSA are most at risk.

3. Methods

This analysis focuses on using open-source datasets to examine the spatial and temporal trends of three climate datasets. The workflow of this analysis mines image collections in Google Earth Engine (GEE), stores the collected data in cloud storage to be compatible in several programs, and is run through a series of statistical and spatiotemporal methods (Fig. 3; See Appendix A.2 Data Automation & Download).

3.1. Datasets

This study utilizes three datasets to examine spatiotemporal trends for the base month of July from 1981 to 2022 across the state of California: the Parameter-elevation Regressions on Independent Slopes Model (PRISM), the Gridded Surface Meteorological (gridMET), and the California Department of Forestry and Fire Protection (CAL FIRE) Wildfire Perimeters.

PRISM is a gridded climate dataset using interpolation techniques to simulate weather and climate across the contiguous United

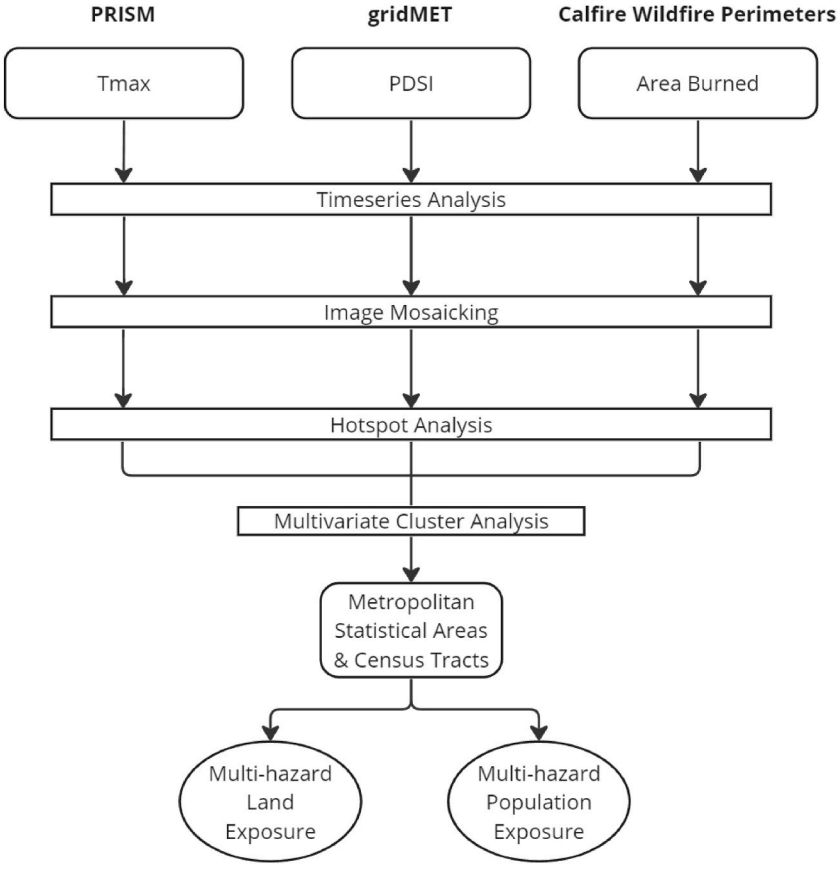

Fig. 3. Workflow for spatiotemporal analysis of multiple hazards to assess land and population exposure.

States [21]. We use the daily maximum temperature (Tmax) available at ~4 km spatial resolution to assess variations of high temperature values in degrees Celsius. Therefore, we utilize daily maximum temperature as the primary heat indicator. The gridMET dataset contains PDSI, capturing relative soil moisture conditions, and has spatial resolution of ~4 km and daily temporal resolution, covering the entirety of the US. PDSI values range from −10 (extreme drought) to +10 (extremely wet) [1]. GridMET is downscaled from station data using physiographic features such as elevation and coastal proximity. The spatial resolution exceeds that of in-situ station observations, enabling comprehensive assessment of variations within and between California's MSAs [58]. CAL FIRE's Wildfire Perimeters is a dataset containing burn areas with their start and end dates from 1879 to 2022 [25]. The dataset does not show the spatial progression of an individual wildfire throughout the event, rather documents the total extent across the start and end dates. While satellite imagery can offer insights to fire progression, we rely on the Wildfires Perimeters dataset as it is the most comprehensive wildfire record in California and widely used for state's policy-making and planning (See Appendix A.3 Pre-processing of Vector Data) [24].

3.2. Temporal analysis

Understanding temporal trends is important because it helps identify patterns and changes over time, which are essential for predicting future risks and planning effective mitigation strategies. By analyzing these trends, we can better understand the progression and severity of hazards. We analyze temporal trends using simple linear regression by calculating the annual averages for each variable and plotting the values against their respective long-term averages. The delineation of the data frames by year allows for calculation of the annual averages for Tmax, PDSI, and wildfire burn area. To calculate the long-term average for Tmax, we obtained the 20th-century average value from NOAA's Climate at a Glance dataset [40]. For PDSI, we rely on the 40-year average from our study period to assess the difference due to the absence of a direct comparison for a 20th-century average. We calculate the average burn area for the 20th century by aggregating July data from 1900 to 2000. Since the total extent of the study area includes several image subsets for smaller regions, we performed image mosaicking (i.e., using the Create Mosaic Raster tool in ArcGIS Pro) to combine the images into a single layer file per variable (See Appendix A.4 Multidimensional Processing).

For the entire study area, we calculated the annual change rate for Tmax, burn area, and PDSI by fitting simple ordinary least squares linear regression models to annual data on each variable.

3.3. Spatial analysis

We examine the spatial trends of individual hazards to understand how they vary across different regions. This is essential for identifying areas that are more prone to each specific hazard. A cluster refers to a group of spatially proximate pixels that exhibit similar hazard patterns, suggesting localized intensities or trends. We calculated the frequency of being an individual hazard cluster for each pixel to identify clusters of values from their spatial and temporal patterns. This is a pixel-based analysis using the K-nearest neighbors method (KNN) which accounts for the surrounding pixels' values; identifying over time, the degree of variance each pixel has experienced. The number of neighbors affects the sensitivity of the analysis. In anticipation of using a KNN method, the optimal number of neighbors was determined as 8 using Moran's I [17].

Using a hotspot analysis allows us to understand the percent of time a hazard significantly impacts a specific pixel location. A hotspot is defined as a statistically significant cluster of high or low pixel values for a particular variable within a spatial dataset. This provides insight into the areas where hazards are most prominent across the state. To determine hotspots, the Getis-Ord Gi* statistic measures the degree of spatial association between neighboring pixels [41]. The Gi* values and their respective statistical significance (P-value <0.05) for each hazard variable indicate where high and low values are spatially clustered for each year. Aggregating the hotspot results across the entire study period, the output we generated by this analysis is the "percent statistically significant hotspot" defined as the proportion of time that a given location (~4 km pixel) experiences a statistically significant high value, measured from 0 to 100. This information provides insights into the temporal stability and persistence of spatial patterns across the study area. Higher percentages in Tmax, PDSI, and wildfire burn areas signify areas of significance or concern. This spatial assessment facilitates the identification of regions experiencing consistent multiple hazards by running the results through multivariate cluster analysis.

3.4. Multivariate cluster analysis

Each result from the hotspot analysis was simultaneously run through a multivariate cluster analysis to identify locations of the percent time of hotspots that exist between Tmax, PDSI, and wildfire burn area. The K-averages algorithm partitions clusters based on the most similar and different features using the Calinski-Harabasz pseudo-F statistic [43,54]. Based on the cluster analysis, the output shows several clusters with low, medium, or high levels for each hazard variable. The levels are identified based on their relative amount of time experienced as a significant hazard hotspot for each cluster. The high levels correspond to those where the hotspot conditions persisted for a larger portion of the time, indicating a more frequent or prolonged co-occurrence of multi-hazard. In total, seven clusters were found in this assessment; we choose the three with the highest percent significance as these are linked to the greatest potential for multiple hazards: 1.) high temperature, high drought, and high wildfire burn area, 2.) high drought and high wildfire, and 3.) high temperature and medium drought.

3.5. Land exposure

We choose California's MSAs as administrative units because they have large concentrations of populations and surrounding land that are prone to these hazards. This assessment takes into account the exposure of the specific MSA to each type of multiple hazard (i.e. 1. high temperature, high drought, and high wildfire occurrence, 2. high drought and high wildfire occurrence, and 3. high temperature and medium drought) results generated by the multivariate cluster analysis.

Using the term land exposure is specifically referring to the amount of space in which a hazard occurs, encompassing all land directly exposed to a hazard [18,31]. This is defined as such to take into account each hazard's direct and indirect impacts. In the case of land exposed to wildfires, this has direct location implications, such as damage to the local ecosystem, as well as indirect implications, such as smoke carrying over to surrounding communities and impacting human health. While land exposed to high temperatures and high drought have mostly direct impacts to land.

To understand the percent of land exposed to each multiple hazard, we overlay the calculated multi-hazard analysis with the MSA dataset. Each multi-hazard area is overlaid and intersected with the area of the MSAs with the resulting data being "cropped" within the boundaries of the MSA. The output results in a table with information from both the MSA and the clusters of multiple hazard data. From there, we compute the area of each type of multiple hazard cluster in acres and use the existing MSA acreages to find the percent of land area exposed and multiply by 100 for the percentage using Equation (1):

$$\%\ land\ exposed = multi - hazard\ area\ within\ the\ MSA\ /\ MSA\ area\ x\ 100 \tag{1}$$

The three resulting outputs (e.i %land exposed to high temperature, drought, and wildfires; %land exposed to high drought and wildfires; %land exposed to high temperature and medium drought) are combined into a single file format to assess the percentage of land exposed to each multiple hazard across all MSAs.

3.6. Population exposure

To calculate population exposure, we utilize Census Tracts containing total population in 2020, from the U.S. Census Bureau [59]. The 26 MSA boundaries have a total of 1702 Census Tracts within them. We use Census Tracts because they are a finer administrative unit and prevent overestimation of population exposure by only intersecting a smaller Census Tract unit rather than the entirety of an MSA.

We then perform a sub-analysis at the Census Tract level and apply it to each multiple hazard cluster. The output from the sub-analysis is a table of Census Tracts that spatially overlap the MSA population totals with each cluster allowing for spatial communication between the two datasets. In this output, only the Census Tracts that intersect with a cluster are included; Census Tracts that do not spatially overlap with a multi-hazard cluster are not included in the output to avoid their population values from contributing to the overall result. From here, we overlay the Census Tracts that contain the intersected cluster information to assign the respective MSA to each Census Tract. We next calculate the percent population exposed (i.e. % population exposed) by dividing the total multi-hazard population exposed (i.e. multi-hazard risk population) by the entire population for each MSA (i.e. MSA total population) and multiply by 100 for the percentage using Equation (2):

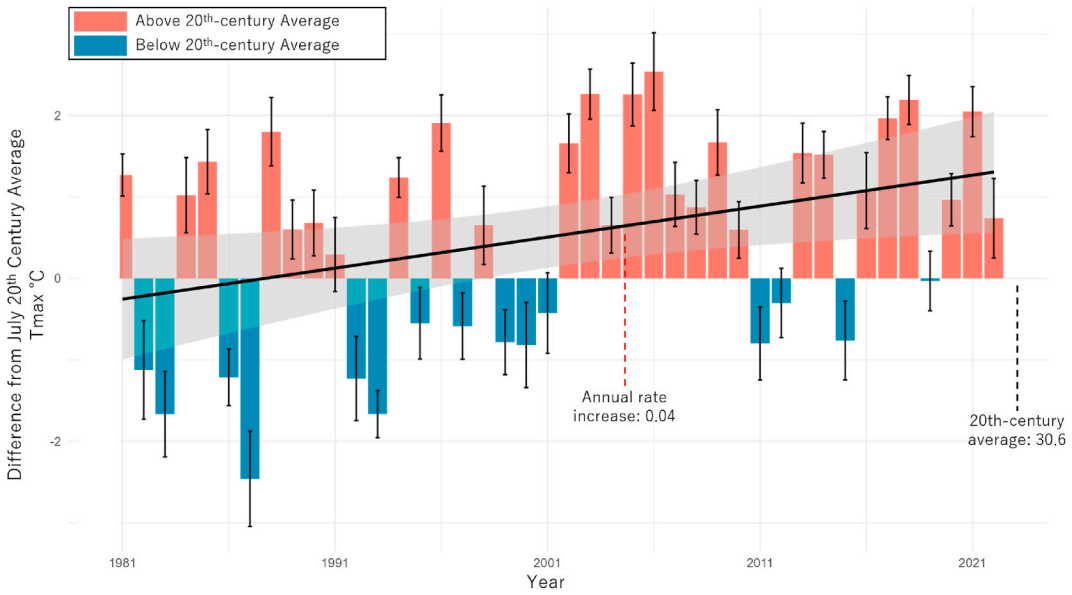

Fig. 4. Tmax July annual average difference from the July 20th century average, measured in degree C. The gray area represents the 95 % confidence interval for the linear regression line.

$$\%\ population\ exposed = multi - hazard\ risk\ population\ within\ the\ MSA\ /\ MSA\ total\ population\ x\ 100 \quad (2)$$

The three resulting outputs are combined into a single file format to assess the percentage of population exposed to each multiple hazard across each of the 26 MSAs.

4. Results

4.1. Each hazard displays increasing trends exceeding long-term average

To illustrate how Tmax, PDSI, and wildfire burn area changes throughout the study period, we use the long-term average for each variable as the baseline and take the difference for each annual average from 1981 to 2022. We take the difference from long-term average to indicate whether a given year in the study was higher or lower in value, allowing for further analysis of each variable's trends.

As expected, Tmax is increasing over time in California (Fig. 4). The Tmax 20th-century average is 30.6 degrees C, with an annual increase rate to be 0.04 degrees C; from 1981 to 2022, there is a total increase of 1.56 degrees C. The overall trend shows a strong increase in the number of years exceeding the 20th-century average, especially seen in the difference of annual average values from 2000 to present. The oscillation from annual averages measuring above and below the 20th-century average diminishes over time, more frequently measuring above the baseline. From 2000, there is a full decade where the annual average for Tmax exceeds the 20th-century average. On average, the state is becoming much warmer and experiencing fewer cooling periods for the month of July.

The results for PDSI follow similar trends to Tmax (Fig. 5). The PDSI annual averages are plotted based on the difference from the PDSI 40-year average (0.16), highlighting the difference in PDSI value above or below the baseline. The regression line shows the annual decrease rate is 0.05, resulting in a total decrease of 2.1 in PDSI value. Following similar trends to Tmax, PDSI shows an overall increase in the number of years measuring below the 40-year average, indicating worsening drought conditions over time. From 2000, we again see a diminishing oscillation of yearly averages recording above and below as a majority of the years record lower than the baseline average. PDSI wet soil conditions are decreasing for the month of July across the study period.

We plot the difference of the percent burn area annual averages of wildfires for July in comparison to the 20th-century average at 0.02 % (Fig. 6). The regression line shows the annual increase rate is 0.04 %, resulting in a total increase of 1.6 % for the study period. In comparison to the annual average trends of Tmax and PDSI, wildfire burn area shows a drastic increase. In the two decades, only six annual averages were recorded below the 20th-century average while the majority of annual averages are far above the baseline. Specifically, July of 2021 experienced a severe spike in the percentage of acres burned, totaling 1.7 million acres. This is equivalent to the size of Santa Barbara County.

4.2. Hotspots of individual hazards

The spatial analysis reveals the hotspots, pixels that have frequently high values, for Tmax, PDSI, and wildfire burn areas across California (Fig. 7). For each variable, the gradient from light to dark represents the amount percent of time a pixel was a significant

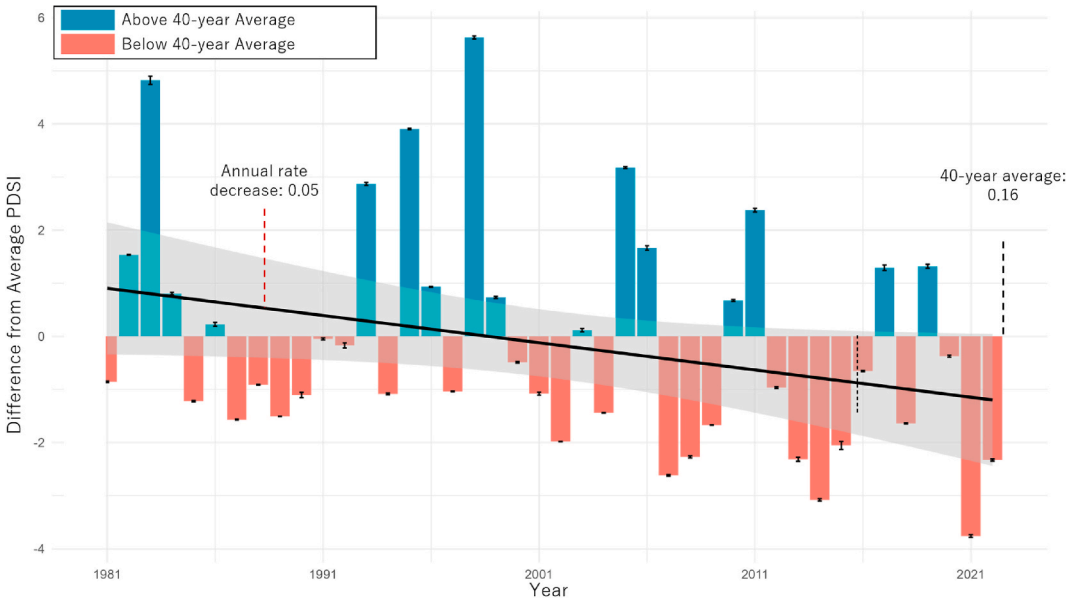

Fig. 5. PDSI July annual average difference from the July 40-year average. The gray area represents the 95 % confidence interval for the linear regression line.

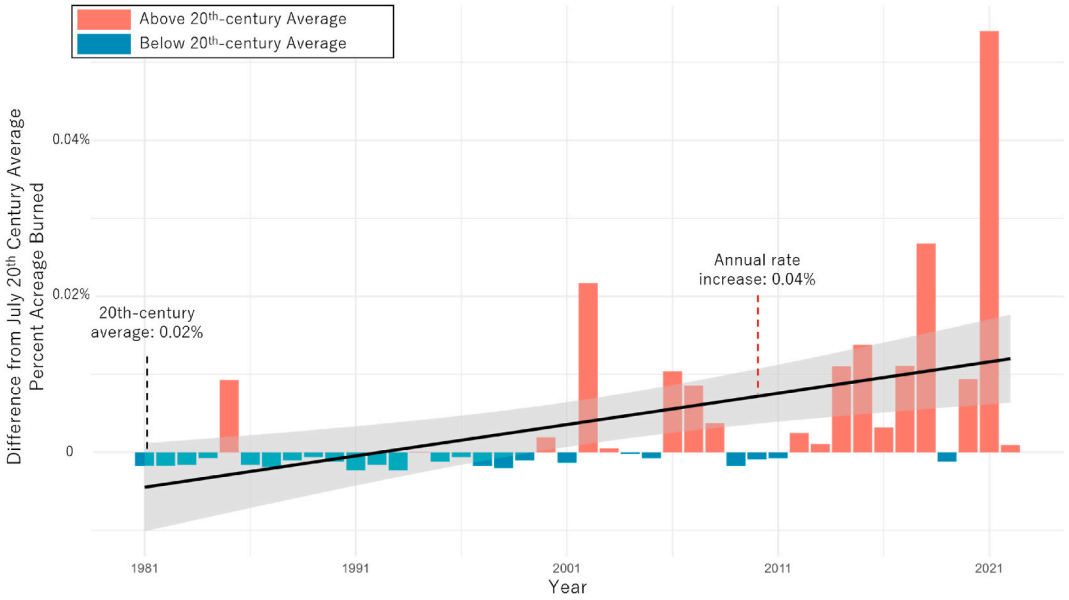

Fig. 6. Wildfire burn area July annual average difference from the July 20th-century average, measured in acres. The gray area represents the 95 % confidence interval for the linear regression line.

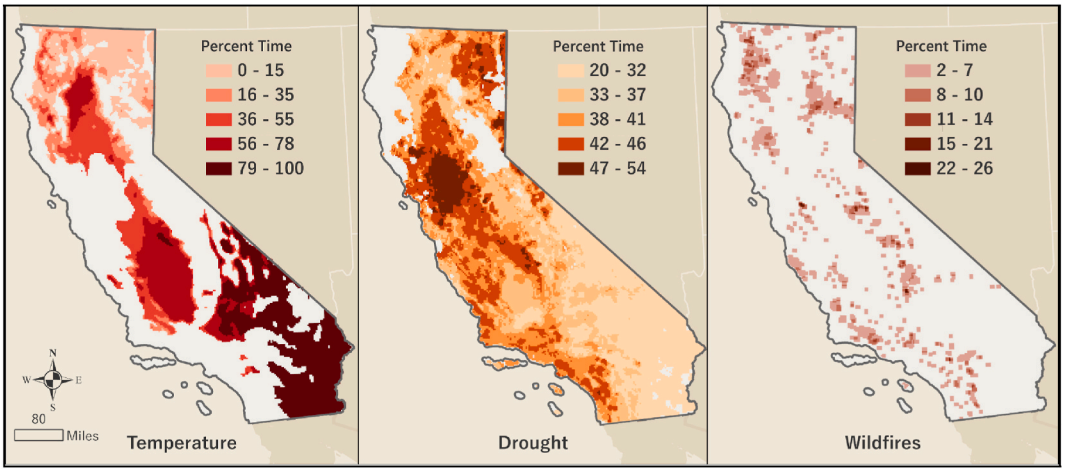

Fig. 7. Pixel frequency as a hotspot from 1981 to 2022 across California for temperature, drought, and wildfires. Gray areas within the study area boundary indicate regions without hazard hotspots.

hotspot from 1981 to 2022.

The hotspots for Tmax are primarily located throughout the Mojave desert (located in southeastern California), Central Valley, and northern California. The hotspots located across California's deserts are expected due to these regions having characteristics of high temperatures and low precipitation to mitigate the high temperatures. In the study period, much of Central Valley and parts of northern California have experienced statistically high values 56–75 % of the time. Surprisingly, there is a lack of hotspots in highly dense urban areas, including the south and central coasts, that are experiencing extreme temperatures [6]. This result, along with the rest of the coast, is most likely attributed to the cooler temperatures from marine influence [8].

Almost the entire state experienced PDSI hotspots for at least 20 % from 1981 to 2022. Drought exhibits high hotspots primarily in northern California, central California, and along the central to southern coastal regions. The north-central region experienced drought conditions for 50 % of the study period.

The presence of wildfires ranges across the entire study area with notable concentrations in the mountainous regions in northern California, border of Central Valley, and interior central to southern coast. The MSAs with the highest percent recurrence of wildfires are San Francisco with 26 %, Bakersfield with 24 %, and Stockton and Riverside-San Bernardino-Ontario with 19 %. As expected, the wildfire trends are almost all located in areas with high drought and mountainous areas.

4.3. Spatial assessment of multiple hazards

The multivariate cluster analysis displays three clusters of multiple hazards across the state (Fig. 8). Each cluster is composed of pixels that frequently experience high values. The red cluster represents high temperature, drought, and wildfire occurrence. This cluster is dispersed across the state and appears in the mountainous areas in northern California, border of Central Valley, and the interior southern coast. The orange cluster includes high drought and high wildfire occurrence-follow an almost identical trend to temperature, drought, and wildfires but encompass more area across the state. The patterns of the red and orange clusters follow along California's hills and mountains ranges which makes sense as the steeper the slope, the faster the fires spread [2]. The yellow clusters are areas of high temperature and medium drought which are located predominantly across Central Valley and southeast regions that border the Mojave desert. As expected, the coastlines do not experience high heat relative to the inland locations, however, this does not dismiss coastal locations as experiencing higher temperatures. These results enable a deeper assessment of the spatial relationships between high-value hazard occurrences within the California MSAs.

4.4. Each MSA has experienced one or more multiple hazard events in the past 40 years

Each MSA in California has experienced a multiple hazard event between 1981 and 2022 with many of these areas experiencing two or more types of multiple hazards (Fig. 9). The percentages in this figure represent the percent of land exposed to a multiple hazard event and the total land in the MSA; for example, over 40 years, 69 % of Bakersfield total land has been exposed to at least one multi-hazard type event. The high temperature, drought, and multi-hazard wildfires show a high percent land exposure along the central to southern coastline MSAs. The high drought and wildfire multi-hazard again follow a similar pattern to high temperature, drought, and wildfires multi-hazard, showing high percent land exposure in the central to southern coast MSAs. In addition, Central Valley MSAs have high percentages of high drought and wildfire multi-hazard events. The high temperature and medium drought multi-hazard displays notably high percent land exposure in varying MSA locations across the state. Taking a closer look at specific MSAs, Bakersfield has surprisingly high land exposure (69 %) while Riverside has relatively medium land exposure (35 %). These two MSAs will be further analyzed in the context of population exposure.

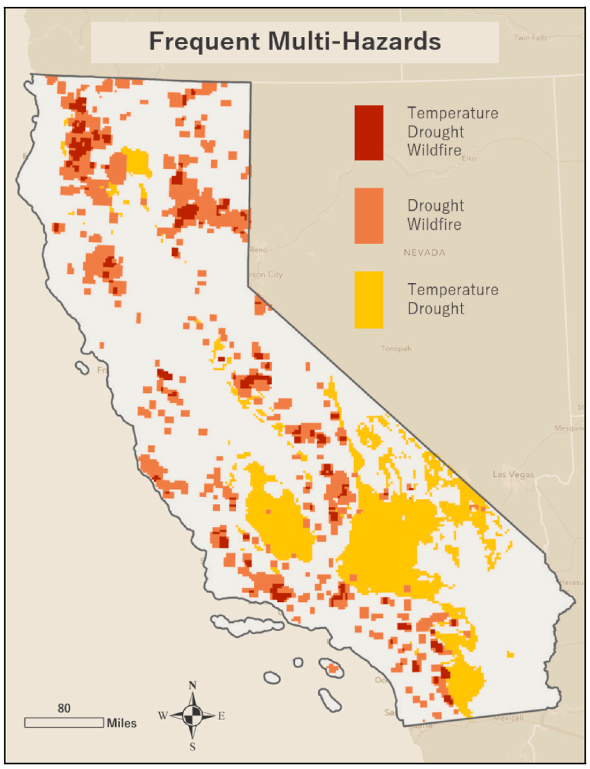

Fig. 8. Multiple hazard hotspots showing locations that have experienced three variations of multiple hazards: 1) high temperatures, drought, and wildfire, 2) high drought and wildfire, and 3) high temperatures and medium drought. Gray areas within the study area boundary indicate regions without multiple hazard hotspots.

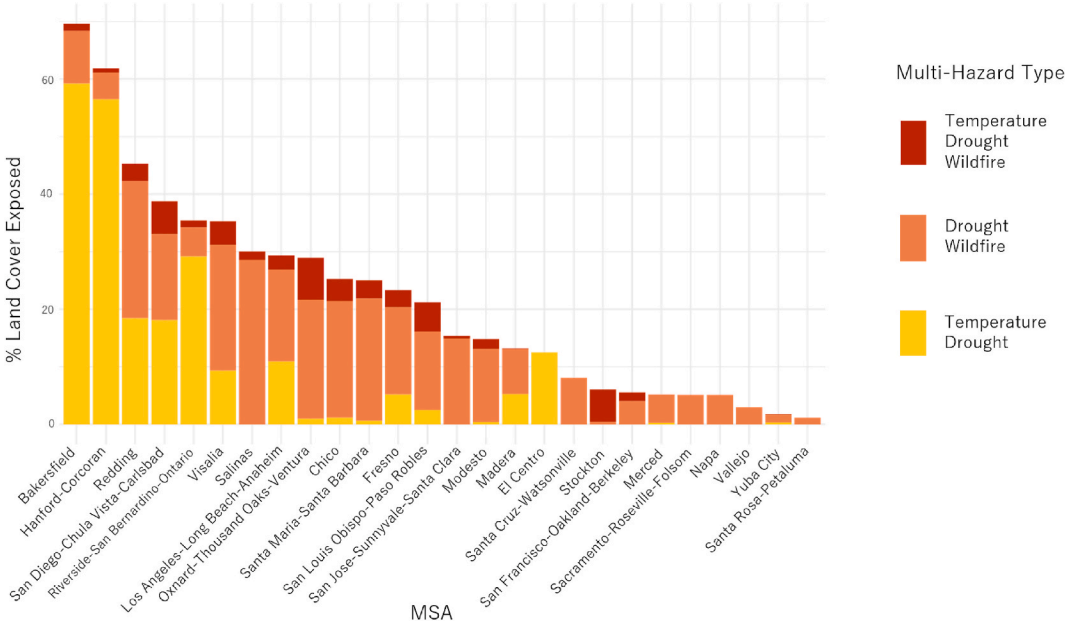

Fig. 9. Percent land cover exposed to each type of multiple hazard per MSA in California for the base month of July from 1981 to 2022. The primary y-axis shows percent of land cover exposed to each multi-hazard type. The MSAs are arranged in order from highest to least count of population exposed.

4.5. Population exposure in California's MSAs

To assess population exposure, we selected MSAs that experience each type of multiple hazard cluster (which includes 15 out of the 26 total MSAs) to understand which cluster has the greatest impact to public health and safety. The primary y-axis shows percent of population is represented by the individual clusters while the secondary y-axis represents the count of population exposed to all multiple hazard clusters in the millions (Fig. 10). The MSAs are arranged in order from highest to least count of population exposed.

Similar to land exposure, Riverside exhibits relatively medium percentages of population exposure to each type of multiple hazards, all under 30 % of the total population. However, the total number of populations exposed surpasses that of all other MSAs. In contrast, Bakersfield shows a higher percentage of population exposed with a comparatively lower number of people affected, just under 1

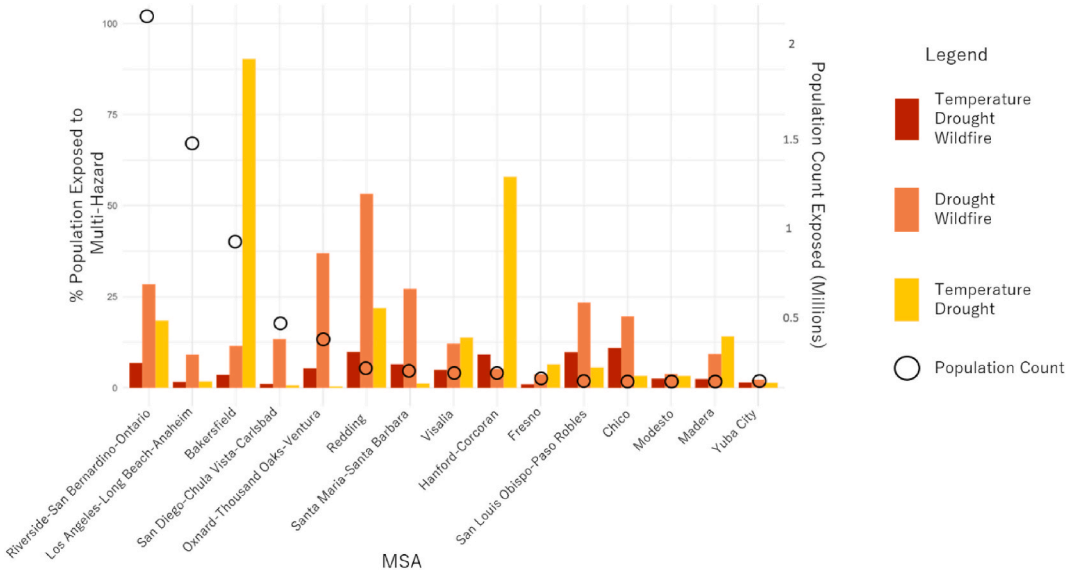

Fig. 10. The percent of population exposed to each type of multiple hazards with the total population count exposed in millions along the dual axis per MSA for the base month of July from 1981 to 2022.

million. In examining the exposure of multiple hazards on MSAs, we find that Riverside and Bakersfield demonstrate contrasting dynamics in population exposure and land cover exposure. When assessing the exposure of urban areas to multiple hazards, it becomes evident that both the percentage of population exposure and the total number of affected individuals are crucial factors to consider.

5. Discussion

5.1. Increasing temporal trends

Our analysis of July from 1981 to 2022 reveals consistent upward trends across temperature, drought, and wildfires. Comparing the annual means with long-term averages exposes a notable increase across the study period. Since 2000, California has experienced more consecutive years above the long-term averages for temperature, drought and wildfires. Reoccurring extreme events reduces the ability for urban systems to recover. Temperature and drought have similar gradual increasing trends while wildfires exhibit severe increases (Figs. 4 and 5). Although 2021 stands out as a significant year in this analysis, it is important to note that 2020 witnessed the most severe fire year on record with 4.3 million acres burned across the state (Fig. 6) [13]. For wildfires, this is especially striking as only 15 % of wildfires in California occur from natural events, highlighting the relevance to anthropogenic impact on hazard occurrence [8]. Analyzing the temporal trends of temperature, drought, and wildfires provides insights into how hazards may be increasing in terms of their spatial extents, intensities, and/or frequencies. This analysis is crucial when considering the way a hazard evolves in their local area and helped to inform this study's spatial assessment.

5.2. Distribution implications of individual hazards

The individual assessment of hazards using hotspot analysis enables us to identify the spatial distribution and frequency of these hazards across the state. Notably, northern California, the central valley, and the central to southern coastal areas for drought and wildfires experience the highest frequency of events (Fig. 7). However, the most unexpected finding from this analysis is the significant occurrence of fires in southern California. Despite recent notable wildfire events in this area, government agencies there are not fully incorporating the wildfire impacts on local populations compared to those in northern California due to lack of resources and stakeholder limitations [57].

Another surprising aspect is the spatial distribution of heat. More frequent occurrences of heat from the individual assessment are not found along the coastlines, despite notable increases. In Southern California's coastal and rural areas, heatwaves have increased in frequency by 46 % and duration by 22 %, especially during drought conditions [33]. Drought affects the entire state, leading to major economic implications and, depending on future scenarios, will continue to impact agricultural communities and contribute to landscape degradation, fueling conditions for wildfires [32]. The correlation between drought and wildfire is very spatially aligned, highlighting specific areas that decision-makers need to focus on. As each hazard increases statewide and spatially overlaps, the potential for multiple hazard events rises, amplifying the probability of their occurrence and the significant damage they can cause. This spatial alignment of hazards, in addition to exposure and vulnerability from other research, points to the need for targeted interventions, to mitigate their impacts effectively [34].

5.3. Distribution implications of multiple hazards

The temporal and spatial analysis of individual hazards across California has provided valuable insights into the state's vulnerability landscape, paving the way for a deeper understanding through multivariate cluster analysis. This analysis is crucial as it highlights both the exact locations and the percentage of time these areas experience various hazards, emphasizing the need to account for multiple hazards rather than just individual ones. For instance, understanding the locations of individual hazards alone misses the interconnectedness of events that collectively contribute to locations with high temperature, drought, and wildfire which is prevalent across the state (Fig. 8).

These hazards pose significant threats to public health, safety, infrastructure, and economic stability in urban areas [45]. The combination of high temperatures, drought, and wildfires not only increases the risk of cardiovascular health issues but also weakens infrastructure and disrupts economic activities [3,27]. The simultaneous impact of multiple hazards can overwhelm response systems, exacerbating challenges faced by communities and decreasing economic stability.

Events defined by significant drought and wildfire occurrences, follow very similar patterns to events with high temperature, drought, and wildfires. This is important for understanding the potential of high drought and wildfire events evolving with the presence of heat in the prevalent areas. Drought and wildfires present severe challenges to the local economy, particularly due to water shortages and land degradation. In 2021, wildfire and drought-related events resulted in a combined disaster cost between 10 and 20 billion USD [40]. Prolonged drought conditions lead to water scarcity, affecting agriculture and residential consumption. Additionally, frequent wildfires damage infrastructure, cause property loss, and disrupt economic stability.

Moderate frequency events, characterized by high temperatures and medium drought occurrences, have similar implications for health, safety, and economic consequences related to water shortages. Despite the absence of wildfires, this combination still poses significant challenges for urban areas, underscoring the importance of assessing both land and population exposure to understand the full extent of vulnerability and prioritize mitigation efforts effectively.

Overall, the findings highlight the interconnected nature of multiple hazard events and their implications for urban vulnerability. Addressing these challenges requires proactive measures to enhance resilience and mitigate the impacts on communities and

economies across California. These insights are essential for enhancing community resilience, mitigating health risks, protecting economic stability, and supporting sustainable development, ultimately informing urban planning and policy decisions to better manage and reduce the risks associated with multiple hazards.

5.4. Importance of discerning land exposure versus population exposure

The comparison of land cover and population exposure across California's MSAs offers valuable insights into the assessment of urban vulnerabilities in the face of multiple hazards. Specifically, when examining areas like Bakersfield and Riverside, significant disparities emerge between the percentage of land exposed versus the percentage of people exposed (Figs. 9 and 10). With this, Riverside experiences a higher population exposure from multiple hazards.

Urban vulnerabilities encompass a range of factors, including infrastructure resilience, human health and safety, and economic stability. In regions such as Bakersfield, known for its significance as an agricultural and energy production hub, high exposure of both land and population carries profound implications not only for local communities but also for broader regions across the nation reliant on their services.

This analysis demonstrates the critical importance of identifying and prioritizing areas that are affected by multiple hazards. By informing decisions regarding the allocation of funding for disaster management and sustainable planning and development, it enables proactive measures to enhance resilience and mitigate the impacts on urban areas and their broader socio-economic networks.

5.5. Limitations and future research

To our knowledge, this is the first study to analyze the multi-hazard clustering of extreme heat, drought, and temperatures with population exposure and land exposure assessments in California. Nevertheless, this study is not without its limitations. First, the methodology focused on the spatiotemporal co-occurrence of these hazards. We did not model the interacting physical processes among them or quantify their cascading effect—such as how prolonged drought conditions may later contribute to widespread wildfires [62,66]. Second, we did not incorporate vulnerability factors beyond population exposure in our risk assessment. Socio-economic variables, such as income, race, education, and immigration status, are well-documented risk factors that influence disaster impacts and recovery costs [20]. Third, urbanization is a key driver of both hazard occurrence and increased exposure, which we did not analyze in this study. For example, the urban heat island effect amplifies extreme heat in densely built environments, while expansion into the wildland-urban interface has increased wildfire risks [44,65]. Lastly, our analysis focuses on July data for each year and all variables in the study, emphasizing broader trends over short-term fluctuations to ensure consistency. While this approach may reduce accuracy in capturing short-term variations such as brief heatwaves or localized weather events, it prioritizes examining long-term patterns of wildfires, extreme heat, and drought conditions over the 40-year period. Future studies investigating the relationship between urbanization and multi-hazard risk could inform climate-resilient urban planning strategies. This study identifies hotspots of multiple hazards across California and raises scientific questions for future research to better understand their drivers and impact.

6. Conclusion

This analysis utilizes spatiotemporal analysis to explore the spatial and temporal co-occurrence between temperature, drought, and wildfires in California. Leveraging high resolution datasets enables a detailed assessment to uncover trends for each variable, which proved invaluable for multiple hazard analyses. Historical data play a vital role in understanding the historical presence of these hazards and anticipating future impacts, as well as identifying previously unrecognized urban vulnerabilities. Understanding the percent of time of individual hazard occurrences, as well as multiple hazard events, is crucial for tracking potential changes that could lead to more drastic increases, as evidenced by California's recent years with fires. By analyzing the temporal patterns of each hazard and their overlaps, we can gain insights into how their impacts are evolving over time. This information is essential for implementing better preparedness and response measures to mitigate the increasing risks associated with these hazards.

Repeated exposure to these hazards exacerbates risk and can lead to severe consequences, further amplifying vulnerabilities in urban systems. As impacts are expected to intensify, comprehending the spatial distribution of multiple hazard events is crucial for identifying and prioritizing sectors most at risk. This analysis highlights the complexities of land exposure versus population exposure to multiple hazards and underscores how the effects of different types of multiple hazards can impact urban vulnerabilities. When incorporating multiple hazards into risk assessments, it is important to understand the spatial relation, temporal relation, and the potential combined impacts to which exact vulnerabilities can be exacerbated by these hazards. This comprehensive understanding enables proactive measures to mitigate risks and enhance resilience in urban areas facing multiple hazards.

CRediT authorship contribution statement

Erin Shives: Writing – review & editing, Writing – original draft, Visualization, Validation, Supervision, Software, Resources, Project administration, Methodology, Investigation, Funding acquisition, Formal analysis, Data curation, Conceptualization. **Tzu-Hsin Karen Chen:** Writing – review & editing, Software, Resources. **C. Karen Seto:** Writing – review & editing, Supervision, Project administration.

Funding sources

This work was supported by the Hixon Center for Urban Sustainability and Yale's Center for Environmental Justice.

Declaration of competing interest

The authors declare that they have no known competing financial interests or personal relationships that could have appeared to influence the work reported in this paper.

Acknowledgements

The lead author is grateful to the California Coastal Commission staff who participated in one-on-one interviews in July of 2023. I am indebted to Joseph G. Toman and Sam W. Wilson for their support throughout the project.

Appendix

A.1) California Population per sq. mile by Census Tract for 2020 [58]

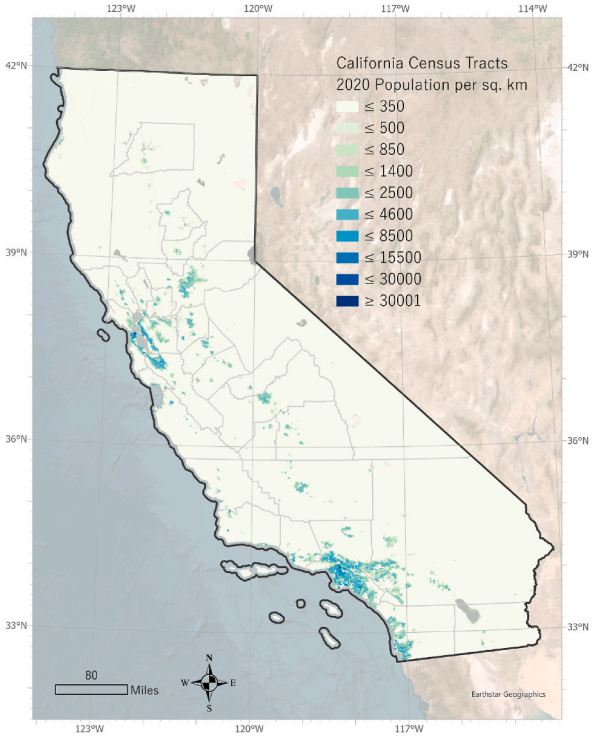

A.2) Data Automation & Download

Downloading datasets with high spatial and temporal resolutions is a major challenge for spatiotemporal analyses. To compensate for this, data mining techniques are often used to detect large datasets [46]. We employ this technique in Google Earth Engine (GEE), a high-performance cloud-computing platform, with a wide variety of available datasets to examine spatiotemporal trends. The batch export function is used to automate the download of hundreds of images to be exported in bulk rather than one image at a time. From here, we download the daily resolution of Tmax (1271 images) and 5-day resolution of PDSI (205 images) for the base month of July from 1981 to 2022 for the entire state of California. Using the bulk download technique does not assign date and time information to output's metadata. To remain organized, each image file name is output with their respective variable and date; for example, Tmax for July 1st, 1981 is tmax_19810701. These data mining techniques allow for a workflow of large, open-source image collection of finer temporal and spatial resolutions.

A.3) Pre-processing of Vector Data

PRISM and gridMET image collections are in raster format while CAL FIRE's Wildfire Perimeters are in vector format. Therefore, the wildfire dataset requires transformation from vector to raster format to be compatible with a space time cube analysis. Start dates in the base month of July are selected to solely account for wildfire activity beginning in this month. All 41 years are batch run through the Polygon-to-Raster tool. The value field is total burnt area in acres, the cell assignment type is cell center and the cell size uses one of the PRISM images to directly match ~4 km spatial resolution. The resulting 41 rasterized wildfire burn area images to allow for comparative analyses.

A.4) Multidimensional Processing

ArcGIS Pro has a suite of tools from the Space Time Pattern Mining toolbox that provide for temporal and spatial assessment of large datasets. The image collections of Tmax, PDSI, and wildfire undergo a series of transformations and analyses to achieve the toolbox's required Network Common Data Form (netCDF) format. The Create Mosaic Raster tool draws from each image collection and combines the images into one layer file per variable. From here, we use the Build Multidimensional Raster Information tool, which embeds date and product information necessary for the program to relate the images to one another across time. This enables the resulting mosaic product to be run through the Make Multidimensional Raster Layer tool, which outputs three multidimensional raster products- Tmax, PDSI, and wildfire burn area. Using these raster products, we use the Create Space Time Cube from Multidimensional Raster Layer tool which arranges the products into the necessary netCDF format to run the Emerging Hotspot Analysis.

Data availability

Data will be made available on request.

References

[1] J.T. Abatzoglou, Development of gridded surface meteorological data for ecological applications and modelling, Int. J. Climatol. 33 (2013) 121–131, https://doi.org/10.1002/2014GL062308. AghaKouchak, A., Cheng, L., Mazdiyasni, O., & Farahmand, A. (2014). Global warming and changes in risk of concurrent climate extremes: Insights from the 2014 California drought: Global Warming and Concurrent Extremes. Geophysical Research Letters, 41(24), 8847–8852.
[2] A. Abouali, D.X. Viegas, J.R. Raposo, Analysis of the wind flow and fire spread dynamics over a sloped–ridgeline hill, Combust. Flame 234 (2021) 111724, https://doi.org/10.1016/j.combustflame.2021.111724.
[3] A. AghaKouchak, F. Chiang, L.S. Huning, C.A. Love, I. Mallakpour, O. Mazdiyasni, H. Moftakhari, S.M. Papalexiou, E. Ragno, M. Sadegh, Climate extremes and compound hazards in a warming world, Annu. Rev. Earth Planet Sci. 48 (1) (2020) 519–548, https://doi.org/10.1146/annurev-earth-071719-055228.
[4] A. AghaKouchak, L. Cheng, O. Mazdiyasni, A. Farahmand, Global warming and changes in risk of concurrent climate extremes: insights from the 2014 California drought: global Warming and Concurrent Extremes, Geophys. Res. Lett. 41 (24) (2014) 8847–8852, https://doi.org/10.1002/2014GL062308.
[5] M.R. Alizadeh, J. Adamowski, M.R. Nikoo, A. AghaKouchak, P. Dennison, M. Sadegh, A century of observations reveals increasing likelihood of continental-scale compound dry-hot extremes, Sci. Adv. 6 (39) (2020) eaaz4571, https://doi.org/10.1126/sciadv.aaz4571.
[6] T.R. Ault, J.S. Mankin, B.I. Cook, J.E. Smerdon, Relative impacts of mitigation, temperature, and precipitation on 21st-century megadrought risk in the American Southwest, Sci. Adv. 2 (10) (2016) e1600873, https://doi.org/10.1126/sciadv.1600873.
[7] J.K. Balch, V. Iglesias, A.L. Mahood, M.C. Cook, C. Amaral, A. DeCastro, S. Leyk, T.L. McIntosh, R.C. Nagy, L. St Denis, T. Tuff, E. Verleye, A.P. Williams, C. A. Kolden, The fastest-growing and most destructive fires in the US (2001 to 2020), Science 386 (6720) (2024) 425–431, https://doi.org/10.1126/science.adk5737.
[8] L. Bedsworth, California's Fourth Climate Change Assessment Statewide Summary Report, vol. 133, 2018.
[9] P.T. Brown, H. Hanley, A. Mahesh, et al., Climate warming increases extreme daily wildfire growth risk in California, Nature 621 (2023) 760–766, https://doi.org/10.1038/s41586-023-06444-3.
[10] M.I. Brunner, C. Chartier-Rescan, Drought spatial extent and dependence increase during drought propagation from the atmosphere to the hydrosphere, Geophys. Res. Lett. 51 (2024) e2023GL107918, https://doi.org/10.1029/2023GL107918.
[11] M. Burke, A. Driscoll, S. Heft-Neal, J. Xue, J. Burney, M. Wara, The changing risk and burden of wildfire in the United States, Proc. Natl. Acad. Sci. USA 118 (2) (2021) e2011048118, https://doi.org/10.1073/pnas.2011048118.
[12] California Department of Fish and Wildlife, Atlas of the Biodiversity of California, California Department of Fish and Wildlife, Sacramento, CA, 2003.
[13] California Department of Forestry and Fire Protection (CAL FIRE), Home - CAL fire, Retrieved from, https://www.fire.ca.gov/our-impact/statistics, 2024.
[14] California Department of Forestry and Fire Protection (CAL FIRE), 2021.
[15] California Remains the World's 5th Largest Economy | Governor of California. (Accessed 7 July 2023).
[16] J.L. Catto, A. Dowdy, Understanding compound hazards from a weather system perspective, Weather Clim. Extrem. 32 (2021) 100313, https://doi.org/10.1016/j.wace.2021.100313.
[17] Y. Chen, Spatial autocorrelation equation based on Moran's index, Sci. Rep. 13 (1) (2023) 19296, https://doi.org/10.1038/s41598-023-45947-x.
[18] Y. Chen, W. Xie, X. Xu, Changes of population, built-up land, and cropland exposure to natural hazards in China from 1995 to 2015, International Journal of Disaster Risk Science 10 (2019) 557–572.
[19] J.N. Claassen, P.J. Ward, J. Daniell, E.E. Koks, T. Tiggeloven, M.C. de Ruiter, A new method to compile global multi-hazard event sets, Sci. Rep. 13 (1) (2023) 13808.
[20] S.L. Cutter, C. Finch, Temporal and spatial changes in social vulnerability to natural hazards, Proc. Natl. Acad. Sci. USA 105 (7) (2008) 2301–2306.
[21] C. Daly, J.W. Smith, J.I. Smith, R.B. McKane, High-resolution spatial modeling of daily weather elements for a catchment in the Oregon cascade mountains, United States, J. Appl. Meteorol. Climatol. 46 (10) (2007) 1565–1586, https://doi.org/10.1175/JAM2548.1.
[22] M.C. De Ruiter, A. Couasnon, M.J. van den Homberg, J.E. Daniell, J.C. Gill, P.J. Ward, Why we can no longer ignore consecutive disasters, Earths Future 8 (3) (2020) e2019EF001425.
[23] G.J. Di Cecco, T.C. Gouhier, Increased spatial and temporal autocorrelation of temperature under climate change, Sci. Rep. 8 (2018) 14850, https://doi.org/10.1038/s41598-018-33217-0.

[24] R. Ferkovich, L. Hartman, J. Johnson, C. Keithley, M. Klaas-Schultz, K. Larvie, R. Marose, E. Meriam, T. Meyer, T. Moody, A. Ong, D. Passovoy, M. Rosenberg, D. Sapsis, J. Spero, N. Tase, D. Tyukayev, R. Walker, D. Bakke, J. Barentson, H. Eng, R. Harris, R. Okusako, K. Pimlott, T. Porter, F. Shilling, J. Thorne, California's forests and rangelands: 2017 assessment. California Department of Forestry and Fire Protection, Fire and Resource Assessment Program, 2018, pp. 85–117. https://frap.fire.ca.gov/assessment2017.

[25] Fire Perimeters CAL FIRE, Fire. https://www.fire.ca.gov/what-we-do/fire-resource-assessment-program/fire-perimeters, 2024. Available at:.

[26] B.E. Flanagan, E.W. Gregory, E.J. Hallisey, J.L. Heitgerd, B. Lewis, A social vulnerability index for disaster management, J. Homel. Secur. Emerg. Manag. 8 (1) (2011), https://doi.org/10.2202/1547-7355.1792.

[27] S. Gao, Y. Wang, Anticipating older populations' health risk exacerbated by compound disasters based on mortality caused by heart diseases and strokes, Sci. Rep. 13 (1) (2023) 16810, https://doi.org/10.1038/s41598-023-43717-3.

[28] J.C. Gill, B.D. Malamud, Hazard interactions and interaction networks (cascades) within multi-hazard methodologies, Earth System Dynamics 7 (3) (2016) 659–679.

[29] S. Greene, S. Kambhampati, C. Shalby, N. Haggerty, Mapping the damage from the Eaton and Palisades fires: Map of damaged buildings in altadena, Los Angeles Times. https://www.latimes.com/california/story/2025-01-16/mapping-los-angeles-damage-from-the-eaton-and-palisades-fires-altadena-pasadena. (Accessed 16 January 2025). Retrieved from.

[30] P. Guerra, Continued Drought Conditions Add Billions in California Agricultural Losses, UC Merced Report Finds | Newsroom, UC Merced News, 2022, November 22. https://news.ucmerced.edu/news/2022/continued-drought-conditions-add-billions-california-agriculture-losses%C2%A0uc-merced-report#:~:text=In%20some%20locations%2C%20crops%20such,shipping%20crops%20out%20of%20California.

[31] B. Güneralp, İ. Güneralp, Y. Liu, Changing global patterns of urban exposure to flood and drought hazards, Glob. Environ. Change 31 (2015) 217–225.

[32] K. Hermans, R. McLeman, Climate change, drought, land degradation and migration: exploring the linkages, Curr. Opin. Environ. Sustain. 50 (2021) 236–244, https://doi.org/10.1016/j.cosust.2021.04.013.

[33] G.C. Hulley, B. Dousset, B.H. Kahn, Rising trends in heatwave metrics across southern California, Earths Future 8 (7) (2020) e2020EF001480, https://doi.org/10.1029/2020EF001480.

[34] IPCC, Climate Change 2022 – Impacts, Adaptation and Vulnerability: Working Group II Contribution to the Sixth Assessment Report of the Intergovernmental Panel on Climate Change, first ed., Cambridge University Press, 2023 https://doi.org/10.1017/9781009325844.

[35] B. Kc, J.M. Shepherd, A.W. King, C. Johnson Gaither, Multiple hazard climate risk projections for the United States, Nat. Hazards 105 (2) (2021) 1963–1976, https://doi.org/10.1007/s11069-020-04385-y.

[36] H.A. Kramer, M.H. Mockrin, P.M. Alexandre, S.I. Stewart, V.C. Radeloff, Where wildfires destroy buildings in the US relative to the wildland–urban interface and national fire outreach programs, Int. J. Wildland Fire 27 (5) (2018) 329, https://doi.org/10.1071/WF17135.

[37] M. Leonard, S. Westra, A. Phatak, M. Lambert, B. van den Hurk, K. McInnes, J. Risbey, S. Schuster, D. Jakob, M. Stafford-Smith, A compound event framework for understanding extreme impacts, WIREs Climate Change 5 (1) (2014) 113–128, https://doi.org/10.1002/wcc.252.

[38] S. Masri, Y. Jin, J. Wu, Compound risk of air pollution and heat days and the influence of wildfire by SES across California, 2018–2020: implications for environmental Justice in the context of climate change, Climate 10 (10) (2022), https://doi.org/10.3390/cli10100145. Scopus.

[39] NBC Los Angeles, Eaton Fire becomes second-most destructive wildfire in California history: through one week the fire northeast of Los Angeles has torched 14,117 acres at 35% containment. https://www.nbclosangeles.com/news/california-wildfires/eaton-fire-most-destructive-california-wildfires/3604825/, 2025, January 14.

[40] NOAA National Centers for Environmental Information (NCEI) U.S, Billion-dollar weather and climate disasters. https://www.ncei.noaa.gov/access/billions/, 2024.

[41] J.K. Ord, A. Getis, Local spatial autocorrelation statistics: distributional issues and an application, Geogr. Anal. 27 (4) (1995) 286–306, https://doi.org/10.1111/j.1538-4632.1995.tb00912.x.

[42] G. Pescaroli, D. Alexander, Understanding compound, interconnected, interacting, and cascading risks: a holistic framework, Risk Anal. 38 (11) (2018) 2245–2257.

[43] R Core Team. (n.d.). R: The R Project for Statistical Computing. Retrieved December 11, 2022, from https://www.r-project.org/.

[44] V.C. Radeloff, D.P. Helmers, H.A. Kramer, M.H. Mockrin, P.M. Alexandre, A. Bar-Massada, V. Butsic, T.J. Hawbaker, S. Martinuzzi, A.D. Syphard, S.I. Stewart, Rapid growth of the US wildland-urban interface raises wildfire risk, Proc. Natl. Acad. Sci. USA 115 (13) (2018) 3314–3319, https://doi.org/10.1073/pnas.1718850115.

[45] C. Raymond, R.M. Horton, J. Zscheischler, O. Martius, A. AghaKouchak, J. Balch, K. White, Understanding and managing connected extreme events, Nat. Clim. Change 10 (7) (2020) 611–621.

[46] K. Rematas, B. Fernando, F. Dellaert, T. Tuytelaars, Dataset fingerprints: exploring image collections through data mining, in: 2015 IEEE Conference on Computer Vision and Pattern Recognition (CVPR), 2015, pp. 4867–4875, https://doi.org/10.1109/CVPR.2015.7299120.

[47] P. Romero Lankao, H. Qin, Conceptualizing urban vulnerability to global climate and environmental change, Curr. Opin. Environ. Sustain. 3 (3) (2011) 142–149, https://doi.org/10.1016/j.cosust.2010.12.016.

[48] J. Rusk, A. Maharjan, P. Tiwari, T.-H.K. Chen, S. Shneiderman, M. Turin, K.C. Seto, Multiple hazard susceptibility and exposure assessment of the Hindu Kush Himalaya, Sci. Total Environ. 804 (2022) 150039, https://doi.org/10.1016/j.scitotenv.2021.150039.

[49] H.D. Safford, A.K. Paulson, Z.L. Steel, D.J.N. Young, R.B. Wayman, The 2020 California fire season: a year like no other, a return to the past or a harbinger of the future? Global Ecol. Biogeogr. 31 (10) (2022) 2005–2025, https://doi.org/10.1111/geb.13498.

[50] F. Schug, A. Bar-Massada, A.R. Carlson, H. Cox, T.J. Hawbaker, D. Helmers, P. Hostert, D. Kaim, N.K. Kasraee, S. Martinuzzi, M.H. Mockrin, K.A. Pfoch, V. C. Radeloff, The global wildland–urban interface, Nature 621 (7977) (2023) 94–99, https://doi.org/10.1038/s41586-023-06320-0.

[51] M. Senande-Rivera, D. Insua-Costa, G. Miguez-Macho, Spatial and temporal expansion of global wildland fire activity in response to climate change, Nat. Commun. 13 (2022) 1208, https://doi.org/10.1038/s41467-022-28835-2.

[52] S.I. Seneviratne, N. Nicholls, D. Easterling, C.M. Goodess, S. Kanae, J. Kossin, Y. Luo, J. Marengo, K. McInnes, M. Rahimi, M. Reichstein, A. Sorteberg, C. Vera, X. Zhang, M. Rusticucci, V. Semenov, L.V. Alexander, S. Allen, G. Benito, F.W. Zwiers, Changes in climate extremes and their impacts on the natural physical environment, in: C.B. Field, V. Barros, T.F. Stocker, Q. Dahe (Eds.), Managing the Risks of Extreme Events and Disasters to Advance Climate Change Adaptation, first ed., Cambridge University Press, 2012, pp. 109–230, https://doi.org/10.1017/CBO9781139177245.006.

[53] N.P. Simpson, K.J. Mach, A. Constable, J. Hess, R. Hogarth, M. Howden, J. Lawrence, R.J. Lempert, V. Muccione, B. Mackey, M.G. New, B. O'Neill, F. Otto, H.-O. Pörtner, A. Reisinger, D. Roberts, D.N. Schmidt, S. Seneviratne, S. Strongin, C.H. Trisos, A framework for complex climate change risk assessment, One Earth 4 (4) (2021) 489–501, https://doi.org/10.1016/j.oneear.2021.03.005.

[54] S.J. Sinaga, N. Satyahadewi, H. Perdana, Determining the optimum number of clusters in hierarchical clustering using pseudo-F, Euler : Jurnal Ilmiah Matematika, Sains Dan Teknologi 11 (2) (2023) 372–382, https://doi.org/10.37905/euler.v11i2.23113.

[55] Z. Stalhandske, C.B. Steinmann, S. Meiler, I.J. Sauer, T. Vogt, D.N. Bresch, C.M. Kropf, Global multiple hazard risk assessment in a changing climate, Sci. Rep. 14 (1) (2024) 5875, https://doi.org/10.1038/s41598-024-55775-2.

[56] S.J. Sutanto, C. Vitolo, C. Di Napoli, M. D'Andrea, H.A.J. Van Lanen, Heatwaves, droughts, and fires: exploring compound and cascading dry hazards at the pan-European scale, Environ. Int. 134 (2020) 105276, https://doi.org/10.1016/j.envint.2019.105276.

[57] S.B. Thapa, J.S. Jenkins, A.L. Westerling, Perceptions of wildfire management practices in a California wildland-urban interface, Environmental Advances 12 (2023) 100382, https://doi.org/10.1016/j.envadv.2023.100382.

[58] U.S. Census Bureau, TIGER/Line shapefile, 2019, nation, U.S., current metropolitan statistical area/micropolitan statistical area (CBSA) national, Retrieved, https://catalog.data.gov/dataset/tiger-line-shapefile-2019-nation-u-s-current-metropolitan-statistical-area-micropolitan-statist, 2019.

[59] U.S. Census Bureau, 2020 Census Tracts, Retrieved from, https://www.census.gov/geographies/mapping-files/time-series/geo/tiger-line-file.2020.html#list-tab-790442341, 2020.

[60] Vereinte Nationen (Ed.), Making Development Sustainable: the Future of Disaster Risk Management, United Nations, 2015.

[61] P.J. Ward, V. Blauhut, N. Bloemendaal, J.E. Daniell, M.C. De Ruiter, M.J. Duncan, R. Emberson, S.F. Jenkins, D. Kirschbaum, M. Kunz, S. Mohr, S. Muis, G. A. Riddell, A. Schäfer, T. Stanley, T.I.E. Veldkamp, H.C. Winsemius, Review article: natural hazard risk assessments at the global scale, Nat. Hazards Earth Syst. Sci. 20 (4) (2020) 1069–1096, https://doi.org/10.5194/nhess-20-1069-2020.
[62] J.C. Witte, et al., NASA A-Train and Terra observations of the 2010 Russian wildfires, Atmos. Chem. Phys. 11 (2011) 9287–9301.
[63] W. Xie, Q. Meng, Spatial and temporal analysis of vulnerability disparity of minorities to wildfires in California, Int. J. Disaster Risk Reduct. 114 (2024) 104949, https://doi.org/10.1016/j.ijdrr.2024.104949.
[64] W. Zhang, M. Luo, S. Gao, W. Chen, V. Hari, A. Khouakhi, Compound hydrometeorological extremes: drivers, mechanisms and methods, Front. Earth Sci. 9 (2021) 673495, https://doi.org/10.3389/feart.2021.673495.
[65] X. Zhou, H. Chen, Impact of urbanization-related land use land cover changes and urban morphology changes on the urban heat island phenomenon, Sci. Total Environ. 635 (2018) 1467–1476.
[66] J. Zscheischler, S. Westra, B.J. Van Den Hurk, S.I. Seneviratne, P.J. Ward, A. Pitman, X. Zhang, Future climate risk from compound events, Nat. Clim. Change 8 (6) (2018) 469–477.